Available online at www.sciencedirect.com
SCIENCE DIRECT®
ELSEVIER
Mechanical Systems and Signal Processing 20 (2006) 718–734
Mechanical Systems and Signal Processing
www.elsevier.com/locate/jnlabr/ymssp

# Gearbox fault diagnosis using empirical mode decomposition and Hilbert spectrum ☆

B. Liu[a,*], S. Riemenschneider[a], Y. Xu[b]

[a]*Department of Mathematics, West Virginia University, P.O. Box 6310, Morgantown, WV 26506-6310, USA*
[b]*Department of Mathematics, Syracuse University, Syracuse, NY 13244, USA*

Received 11 February 2004; received in revised form 19 January 2005; accepted 7 February 2005
Available online 16 April 2005

**Abstract**

The empirical mode decomposition (EMD) and Hilbert spectrum are a new method for adaptive analysis of non-linear and non-stationary signals. This paper applies this method to vibration signal analysis for localised gearbox fault diagnosis. We first study the properties of the recently developed B-spline EMD as a filter bank, which is helpful in understanding the mechanisms behind EMD. Then we investigate the effectiveness of the original and the B-spline EMD as well as their corresponding Hilbert spectrum in the fault diagnosis. Vibration signals collected from an automobile gearbox with an incipient tooth crack are used in the investigation. The results show that the EMD algorithms and the Hilbert spectrum perform excellently. They are found to be more effective than the often used continuous wavelet transform in detection of the vibration signatures.


## 1. Introduction

Fault diagnosis of gearboxes is of crucial importance and has been studied for several decades. A distinct characteristic of gearbox faults is that they often generate vibration signals with amplitude and/or phase modulation. In the frequency domain, this is reflected by the increase of

☆Supported in part by National Aeronautics and Space Administration under Grant NAG5-5364, and National Science Foundation under Grants NSF0314742 and NSF0312113.
*Corresponding author.
*E-mail address:* bliu@math.wvu.edu (B. Liu).

0888-3270/$ - see front matter © 2005 Elsevier Ltd. All rights reserved.
doi:10.1016/j.ymssp.2005.02.003

the sideband components around the related meshing frequencies and their harmonics [1]. In general, a fault that has distributed effects, such as gear eccentricity, generates only a few sideband components. Spectral analysis is usually effective in detection of such faults. In contrast, a localised fault such as tooth crack excites transients into the background vibration, which results in a sequence of sideband components in the spectrum. In the early development stage of the localised faults, the sideband components are not easy to recognise from the spectrum because they are distributed in broad frequency bands and may overlap with some background components.

Time domain averaging may be the most popular traditional technique [1] for detection of the localised faults. It is powerful in suppressing the noise and other non-synchronous components but has the limitation that it usually requires a reference signal for synchronising the averaging. A significant recent development in gearbox diagnosis is the application of time–frequency analysis. It is capable of revealing the time–dependent spectrum of a signal over the full frequency extent and therefore can overcome to a great extent the drawbacks of the traditional techniques. So far, the most studied time–frequency analysis approach in gearbox fault diagnosis is wavelet transform. It has been shown to be relatively effective in revealing the vibration transient features of a gearbox with localised faults (see [2] for details).

However, the traditional time–frequency analysis techniques each have their own limitations [3]. To improve the technology, Huang et al. [4] proposed a new method. This method decomposes a signal using the so-called empirical mode decomposition (EMD) into a finite sum of components known as intrinsic mode functions (IMF). It then applies the Hilbert transform to the IMFs to obtain a time–frequency representation called the Hilbert spectrum. A breakthrough of this method is that as opposed to the traditional time–frequency analysis techniques, it does not use pre-specified basis functions or filters but instead decomposes a signal by direct extraction of the local energy associated with the intrinsic time scales of the signal itself. It is therefore highly adaptive and consequently can well depict the time–frequency characteristics of a signal. This method is now known as the Hilbert–Huang transform (HHT) in the literature. It has been proved remarkably effective in various applications, e.g., [5–7]. Recently, the last two authors of the present research and their collaborators [8] proposed a B-spline approach for empirical mode decomposition (BS-EMD). This approach, as discussed in [8], is more amenable for dealing with the mathematical problems related to the HHT.

The purpose of the present research is two-fold. The first is to improve the diagnosis of localised gearbox faults by using the HHT including both the original and the B-spline EMD. The second is to examine the performance of the BS-EMD in dealing with practical problems, which in turn will be helpful for the further mathematical study on the HHT. In Section 2, the original and the B-spline EMD methods are reviewed briefly. Then in Section 3, we study the properties of the B-spline EMD as a filter bank, which is of interest to both theoretical study and applications. In Section 4, we apply the two EMD methods and the Hilbert spectrum to the detection of a gear tooth crack and compare their performances with that of the continuous wavelet transform. The conclusion is presented in Section 5.

## 2. Empirical mode decomposition

### 2.1. The original EMD

The EMD method was motivated by computation of instantaneous frequency defined in terms of Hilbert transform. As is well known, for a real-valued signal $x(t)$, the Hilbert transform is

defined by the principal value (PV) integral [9]

$$y(t) = \frac{1}{\pi} PV \int_{-\infty}^{\infty} \frac{x(\tau)}{t-\tau} \, d\tau. \tag{1}$$

This leads to the definition of an analytic signal

$$z(t) = x(t) + iy(t) = a(t)e^{i\theta(t)}, \tag{2}$$

where

$$a(t) = [x^2(t) + y^2(t)]^{1/2}, \quad \theta(t) = \arctan\frac{y(t)}{x(t)}. \tag{3}$$

The instantaneous frequency is then defined by

$$\omega(t) = \frac{d\theta(t)}{dt}. \tag{4}$$

In the above process, both the amplitude and instantaneous frequency are a function of time. One would therefore hope to construct a time–frequency representation based on Hilbert transform. In [4], Huang et al. showed that for a function to have physically meaningful instantaneous frequency, it should satisfy: (1) the number of the extrema and the number of the zero crossings are equal or differ at most by one, and (2) at any point, the mean value of the envelopes defined by the local extrema is zero. Such a function is called an IMF. A practical signal is usually not an IMF but using the EMD, the signal can be decomposed into a finite sum of IMFs [4].

Denote by $x(t)$ the signal to be analysed. The EMD extracts the first IMF by the following sifting process:

1. Find the upper envelope of $x(t)$ as the cubic spline interpolant of its local maxima, and the lower envelope, as the cubic spline interpolant of its local minima.
2. Compute the envelope mean $m(t)$ as the average of the upper and lower envelopes.
3. Compute $h(t) = x(t) - m(t)$.
4. If the sifting result $h(t)$ is an IMF, stop. Otherwise, treat $h(t)$ as the signal and iterate on $h(t)$ through Steps 1–4. The stopping condition is

$$\sum_t \frac{[h_{k-1}(t) - h_k(t)]^2}{h_{k-1}^2(t)} < SD, \tag{5}$$

where $h_k(t)$ is the sifting result in the $k$th iteration, and $SD$ is typically set between 0.2 and 0.3.

The EMD extracts the next IMF by applying the above procedure to the residue $r_1(t) = x(t) - c_1(t)$, where $c_1(t)$ denotes the first IMF. This process is repeated until the last residue $r_n(t)$ has at most one local extremum.

The above procedure decomposes the original signal as a finite sum of IMFs $c_j(t)$, $j = 1, \ldots, n$. Applying the Hilbert transform to each IMF, we obtain the analytic signal of $x(t)$

$$z(t) = \sum_{j=1}^{n} a_j(t) \exp\left( i \int_{-\infty}^{t} \omega_j(\tau) \, d\tau \right). \tag{6}$$

One can then represent the signal energy as a joint function of time and the instantaneous frequency. Such a representation is called Hilbert spectrum. The residue $r_n(t)$ characterises the trend of the signal and is treated separately.

### 2.2. The B-spline EMD

The BS-EMD was developed for the convenience of studying the mathematical foundation of the general EMD method, such as the convergence of the EMD algorithm. In the present research, we will focus on investigating the performance of this method in processing practical data. For more details on the algorithmic and mathematical discussion, the reader is referred to [8].

We first give the definition of B-splines [10]. A B-spline $B_{j,k}(t)$ is a piecewise polynomial of order $k$ with knots $\tau_j, \ldots, \tau_{j+k}$. It is positive on the interval $(\tau_j, \tau_{j+k})$ and zero outside this interval. Specifically, for a given increasing sequence of knots $\tau_j$, $j \in Z$, the $j$th B-spline of order $k$ is obtained by

$$B_{j,k}(t) = \frac{t - \tau_j}{\tau_{j+k-1} - \tau_j} B_{j,k-1}(t) + \frac{\tau_{j+k} - t}{\tau_{j+k} - \tau_{j+1}} B_{j+1,k-1}(t) \tag{7}$$

with

$$B_{j,1}(t) = \begin{cases} 1, & \tau_j \leqslant t < \tau_{j+1}, \\ 0, & \text{elsewhere.} \end{cases} \tag{8}$$

Fig. 1 shows a cubic B-spline, for which $k = 4$.The segment between every two neighbouring knots is a polynomial of degree 3.

In the BS-EMD, the knots of the B-splines are taken as the local extremum points of the signal $x(t)$ and the envelope mean in the original EMD is replaced with the moving average of B-splines [8]. Particularly, for $k = 4$, which is the case used in the present research, we have the moving average as the linear combination of cubic B-splines

$$m(t) = \sum_{j \in Z} \frac{1}{4} [x(\tau_{j+1}) + 2x(\tau_{j+2}) + x(\tau_{j+3})] B_{j,4}(t), \tag{9}$$

where $x(\tau_{j+1})$, $x(\tau_{j+2})$ and $x(\tau_{j+3})$ are the $(j+1)$th to $(j+3)$th local extrema of $x(t)$, and the knots of $B_{j,4}(t)$ are $\tau_j, \tau_{j+1}, \ldots, \tau_{j+4}$, the $t$-coordinates of the $j$th to $(j+4)$th local extrema.

After the above modifications, we obtain the BS-EMD algorithm. This algorithm extracts the first IMF from the signal $x(t)$ as follows:

1. Find the local extrema of $x(t)$.
2. Compute the moving average $m(t)$ (using Eq. (9) for cubic B-splines).
3. Compute $h(t) = x(t) - m(t)$.
4. If the sifting result $h(t)$ is an IMF, evaluated using Eq. (5), stop. Otherwise, treat $h(t)$ as the signal and iterate on $h(t)$ through Steps 1–4.

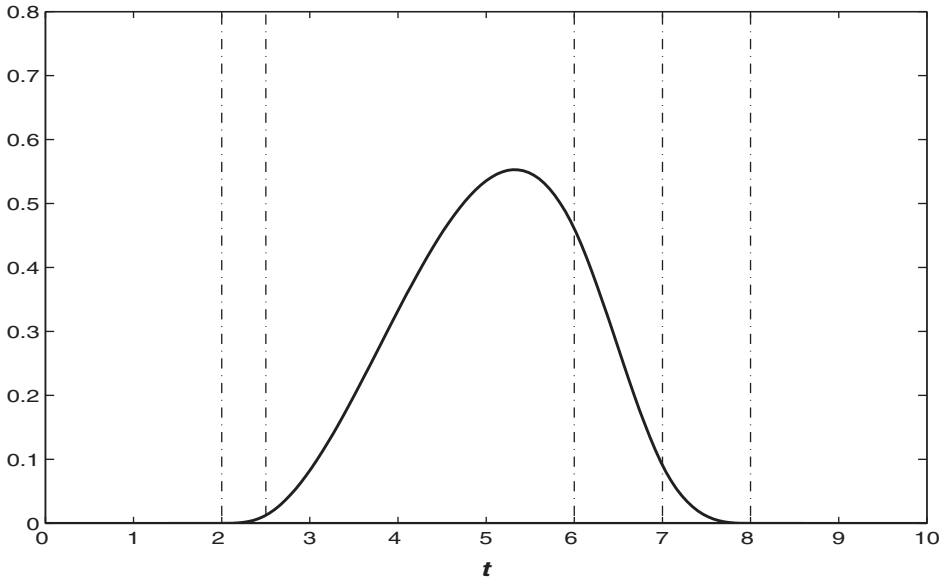


Fig. 1. Cubic B-spline of knots $t = 2, 2.5, 6, 7, 8$. Each segment between the neighbouring vertical dash–dot lines, which across the knots on the horizontal axis, is a polynomial of degree 3.

The algorithm proceeds to select the next IMF by applying the above procedure to the first residue $r_1(t) = x(t) - c_1(t)$, and repeats the process until the last residue $r_n(t)$ has at most one local extremum. We can then apply the Hilbert transform to each IMF to obtain the Hilbert spectrum.

## 3. B-spline EMD as a filter bank

In this section, we study the properties of the B-spline EMD as a filter bank. This is of importance for its application and helpful for understanding its performance.

In [11,12], it has been shown numerically that the original EMD acts as a filter bank resembling that involved in the dyadic wavelet transform [3]. To understand the behaviour of the BS-EMD in this respect, the following numerical experiment is carried out. First, we generate 3000 independent Gaussian white-noise time series of length 1024. Each of them is decomposed using the cubic B-spline EMD. Corresponding to each mode of the decomposition, the IMF is windowed and Fourier transformed. The power spectrum for each mode is then estimated as the average of the squared absolute values of the corresponding Fourier transforms over all the realisations. The result is presented in Fig. 2(a), where each profile corresponds to one decomposition mode. The collection of all the profiles can be interpreted as the frequency output of an equivalent filter bank. For comparison, Fig. 2(b) presents the power spectra obtained from the original EMD using the same procedure. It can be seen that, similarly to the original EMD, the B-spline EMD also behaves closely to a dyadic filter bank.

To interpret the above filter bank property of the B-spline EMD, let us consider a signal composed of a high-frequency sinusoid riding on a low-frequency sinusoid, as shown in Fig. 3(a), where the local extrema are marked by "o".

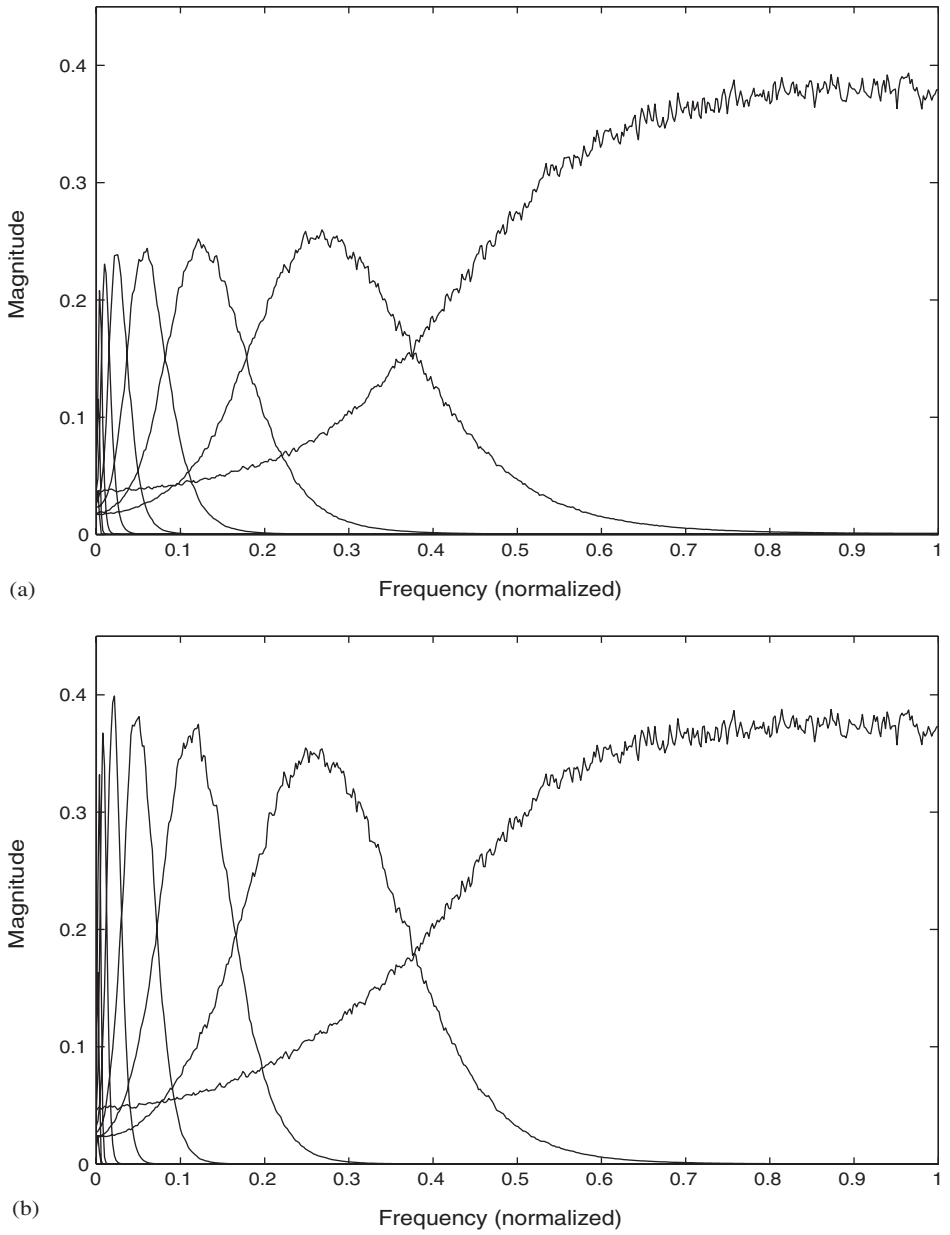


Fig. 2. Power spectra of the IMFs obtained using (a) the BS-EMD and (b) the original EMD. The IMF index increases from the right to the left.

Let $p_j$ be the coefficient of the B-spline $B_{j,4}(t)$ in Eq. (9), that is, $p_j = \frac{1}{4}[x(\tau_{j+1}) + 2x(\tau_{j+2}) + x(\tau_{j+3})]$. Then, $\{p_j\}$ as a sequence in $j$ is essentially the output of a low-pass filter $\{\frac{1}{4}, \frac{1}{2}, \frac{1}{4}\}$ applied to the local extremum sequence. In other words, the coefficient sequence of the B-splines is a smoothed version of the local extremum sequence and represents the low-frequency part of the

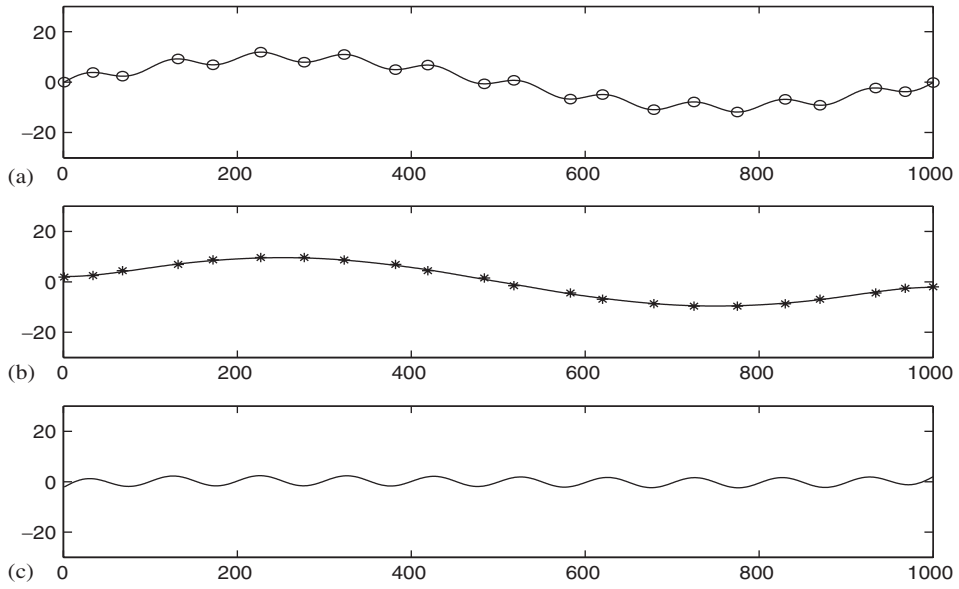


Fig. 3. (a) A signal composed of a high-frequency sinusoid riding on a low-frequency sinusoid, where the local extrema are marked by "o". (b) The points "*" represent the cubic B-spline coefficients. The waveform is obtained using Eq. (9). (c) The difference between the signal and the waveform in (b).

latter. This can be seen from Fig. 3(b), where the B-spline coefficients represented by "*" have obviously less oscillation than the local extremum sequence represented by "o" in Fig. 3(a).

Furthermore, in [10], it is proved that a function represented in the form of Eq. (9) does not have more sign changes than the coefficient sequence $\{p_j\}$ itself. We may thus consider that the component represented by Eq. (9) is the low-frequency part or the local mean of the signal. In Fig. 3(b), the waveform shows such a low-frequency part of the signal in Fig. 3(a). The high-frequency part obtained by subtraction of the low-frequency part from the signal is shown in Fig. 3(c).

In the next iteration of the sifting process, a new low-frequency part is generated from the current high-frequency part. When the stopping condition is satisfied, we obtain a high-frequency part, i.e. the first IMF, and the difference between the signal and the IMF. It can be easily shown that this difference is equal to the sum of the low-frequency parts generated in all the iterations of the sifting process. The next IMF is extracted in the same way but from this difference. One can imagine that when all the IMFs are obtained, the signal will be decomposed into a number of frequency bands similar to the situation of wavelet transform.

## 4. Detection of gear tooth crack

In this section, we apply the original and the B-spline EMD methods to the detection of gear tooth crack. The vibration signals used in the study were collected from an experiment conducted on an automobile gearbox. The transmission path was: $Z28/Z48 \rightarrow Z20/Z44 \rightarrow Z30/Z36 \rightarrow$

$Z15/Z42$, where each fraction represents one gear pair, the number following $Z$ in the numerator is the number of teeth of the driving gear and that in the denominator is the number of teeth of the driven gear. In the experiment, the input shaft was kept running at 1600 rpm and a full load was applied to the output shaft. The vibration signals were picked up at the bearing seat of the output shaft. They were low-pass-filtered at 1.8 kHz and digitised at the sampling frequency of 4 kHz. During the experiment, one tooth of the driving gear ($Z15$), which ran at 5.89 Hz, in the last meshing pair was found broken. Fig. 4 shows a signal collected immediately after the breakage happened, which contains large transients spaced regularly in time. Our purpose is to diagnose the fault from the vibration signals collected before the tooth was broken. During that stage, a crack would be developing, which would excite a sequence of small transients into the background vibration.

For good observation of the featured vibration components, we will use the smoothed Hilbert spectrum throughout this section. The smoothed Hilbert spectrum here is obtained by applying a $21 \times 41$ smoothing Gaussian filter to the original Hilbert spectrum [4]. Also, in order to compare the details of the results of different methods, in all the grey-scale time–frequency representations, we show only the frequency band from 0 to 1 kHz (the Nyquist frequency is 2 kHz). This frequency band covers the frequencies of interest in all the analyses.

We first analyse a signal picked up 1 min before the tooth was broken. The waveform and the Fourier transform of the signal are presented in Fig. 5. Fig. 6(a) shows the first seven IMFs obtained using the BS-EMD (the rest were found unimportant for the present fault diagnosis problem). One can see that IMFs 3–6 contain equally spaced transients. To find out the frequency range of the transients, we compute the Hilbert spectrum from these four IMFs. Fig. 6(b) presents the result, where the relatively dark patches show the time–frequency characteristics of the

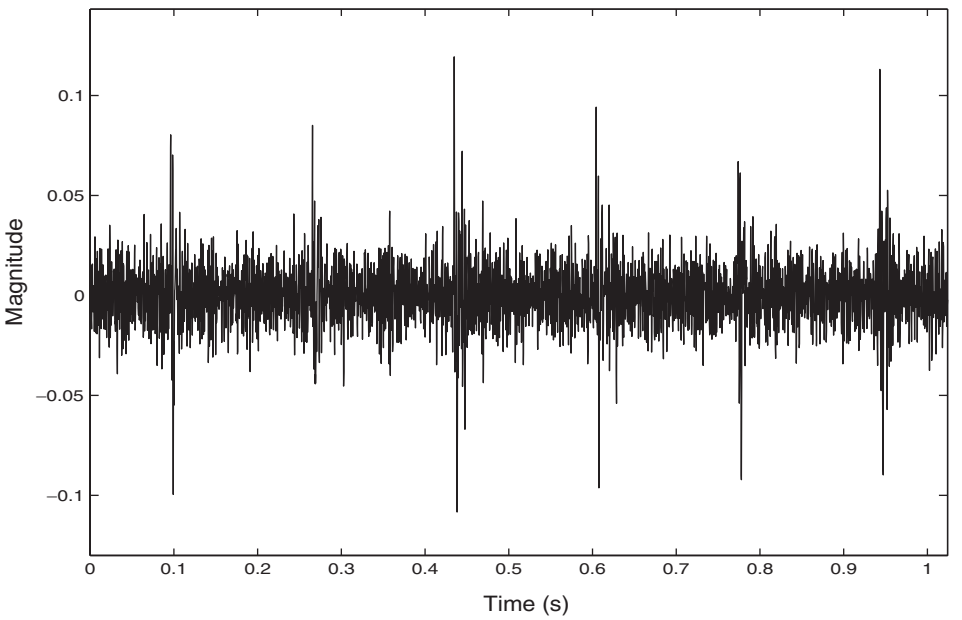


Fig. 4. A vibration signal collected immediately after the gear tooth was broken.

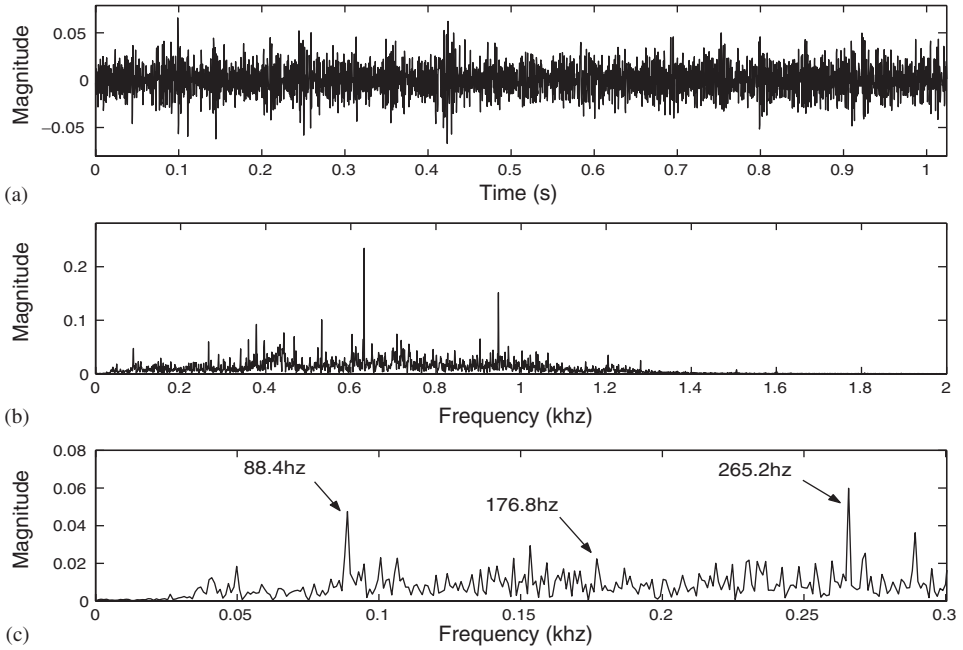


Fig. 5. (a) A vibration signal collected 1 min before the tooth was broken, (b) its Fourier transform, and (c) the zoomed-in plot of the Fourier transform from 0 to 0.3 kHz.

transients. From Fig. 6, we can obtain the following information. Firstly, the average time spacing between the neighbouring impulses is about 0.17 s. It is 5.9 Hz in frequency, which is close to the rotation frequency of the damaged gear. Secondly, the frequencies of the transients range from 0 to about 300 Hz. This covers the sidebands of the meshing frequency of the last gear pair in the transmission path, which is about 88.4 Hz, and the sidebands of the second and third harmonics of the meshing frequency, which are 176.8 and 265.2 Hz, respectively. These features indicates clearly the existence of a localised defect on the driving gear of the last gear pair.

From the zoomed-in plot of the Fourier transform shown in Fig. 5(c), one can see that there exist a number of sideband components around the indicated meshing frequency and its second and third harmonics. Particularly, the frequency spacing between the peaks of the major sideband components of the meshing frequency and its third harmonic is about 6 Hz, which is close to the rotation frequency of the damaged gear. This does indicate the possible existence of a localised defect on the gear [1]. However, compared with Fig. 6, the IMFs and Hilbert spectrum provide much more direct and explicit information about the fault. In fact, as will be seen in the second example given later, it is rather difficult to recognise the defect from the Fourier transform when the transient is very small.

Figs. 7(a) and (b) show the first seven IMFs and the Hilbert spectrum of IMFs 3–6 obtained using the original EMD. It appears that the Hilbert spectrum here provides the information similar to Fig. 6(b). However, for this specific signal, the IMFs obtained using the BS-EMD reveal the transients better than those obtained using the original EMD.

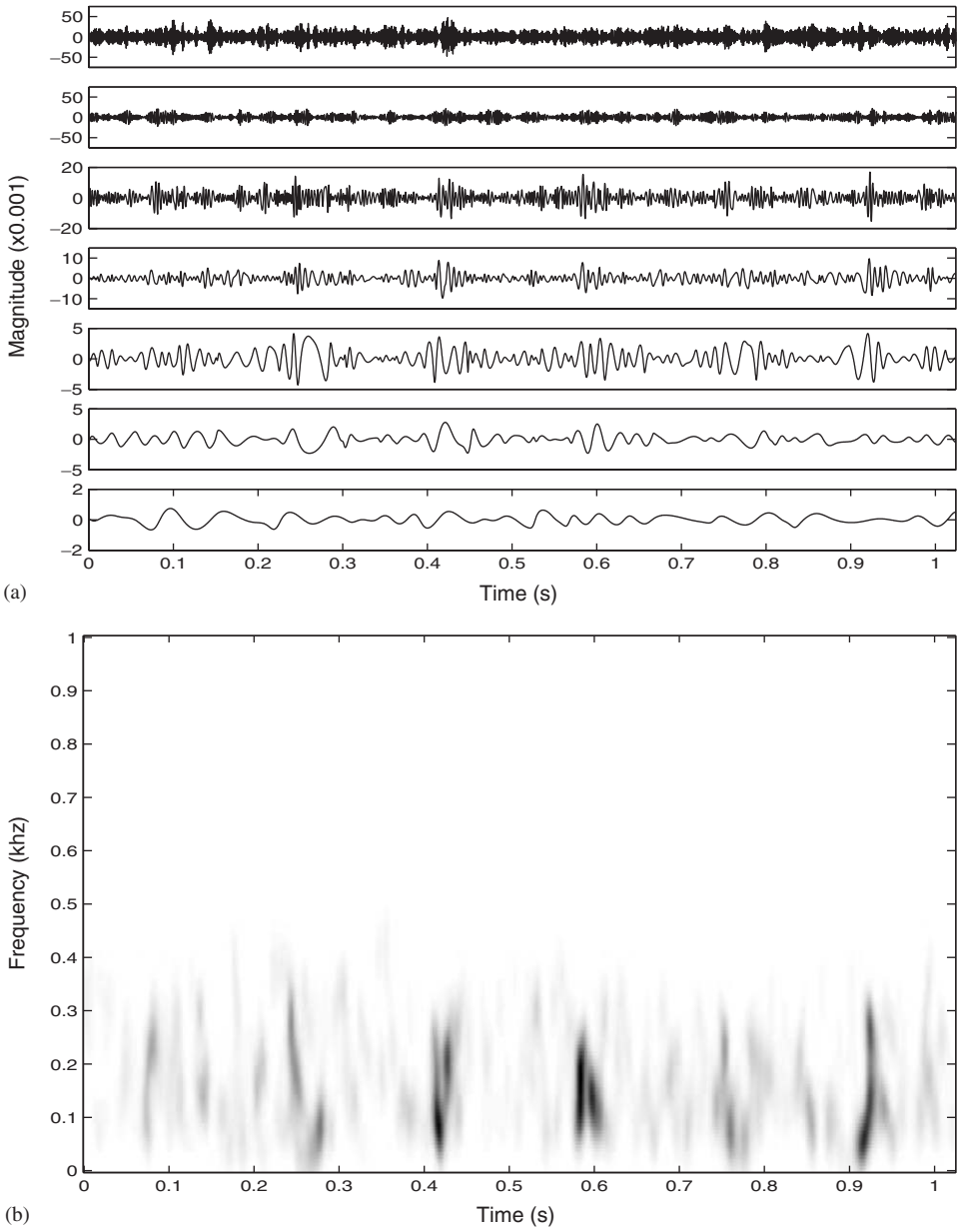


Fig. 6. (a) IMFs of the signal in Fig. 5(a) obtained using BS-EMD. The index of the IMF increases from the top to the bottom. (b) Hilbert spectrum of the 3rd–6th IMFs.

For comparison, we also analyse the signal using the continuous wavelet transform, which is the most studied wavelet method in gearbox diagnosis. The complex Morlet wavelet [3] $w(t) = \frac{1}{\sqrt{2\pi}} \exp\left(\frac{-t^2}{2}\right) \exp(i2\pi t)$ is used in the analysis. Fig. 8(a) shows the real parts of the CWT at the seven dyadic scales from $a = 1$ to 64. One can see that the 5th to 7th waveforms, corresponding to

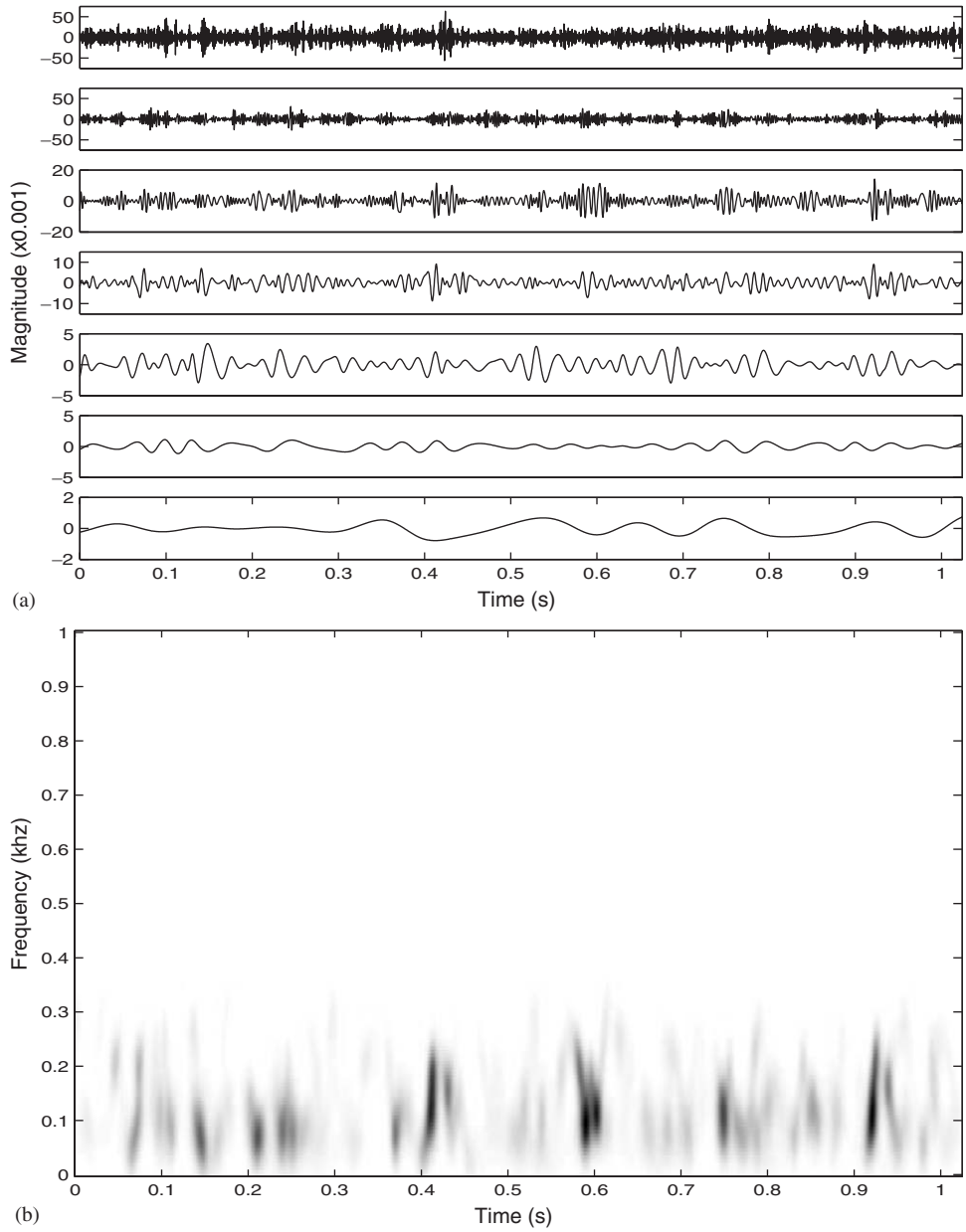


Fig. 7. (a) IMFs of the signal in Fig. 5(a) obtained using the original EMD. The index of the IMF increases from the top to the bottom. (b) Hilbert spectrum of the 3rd–6th IMFs.

scales $a = 16$, 32 and 64 reveal the transients clearly. Fig. 8(b) gives the CWT time–frequency representation of the signal. In the frequency band from about 100 to 300 Hz, the representation can well characterise the time–frequency distribution of the transients. However, for the sidebands below the meshing frequency 88.4 Hz, the sharp structures of the transients are smoothed and

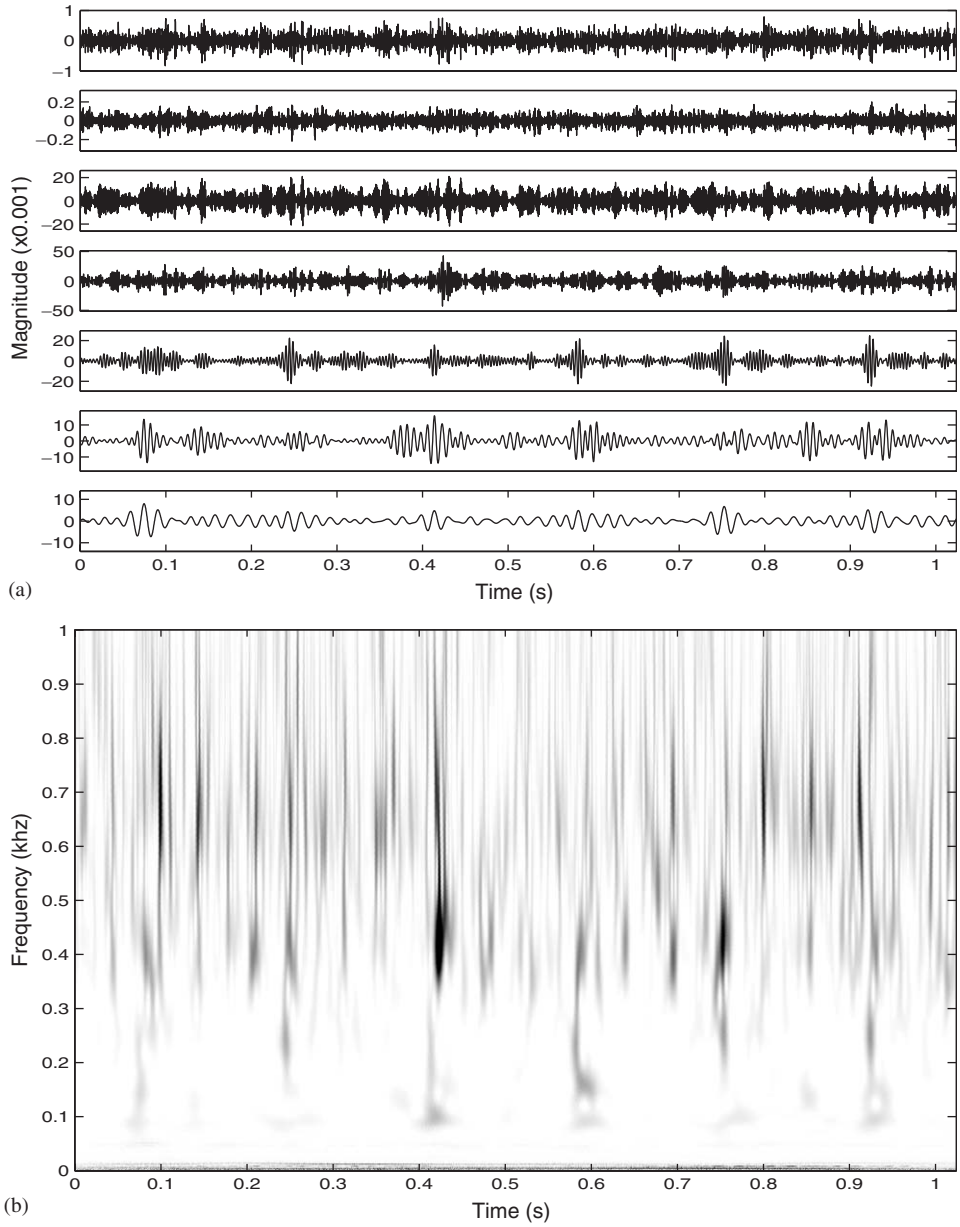


Fig. 8. (a) CWT of the signal in Fig. 5(a) at the dyadic scales from $a = 1$ (top) to 64 (bottom). (b) CWT time–frequency representation.

become less noticeable. This is because the wavelets at these frequencies have relatively large scales and the energy of the transients is spread.

Now we analyse a signal collected 6 min before the tooth was broken, for which the transients are much less obvious. The waveform and its Fourier transform are shown in Fig. 9. For this

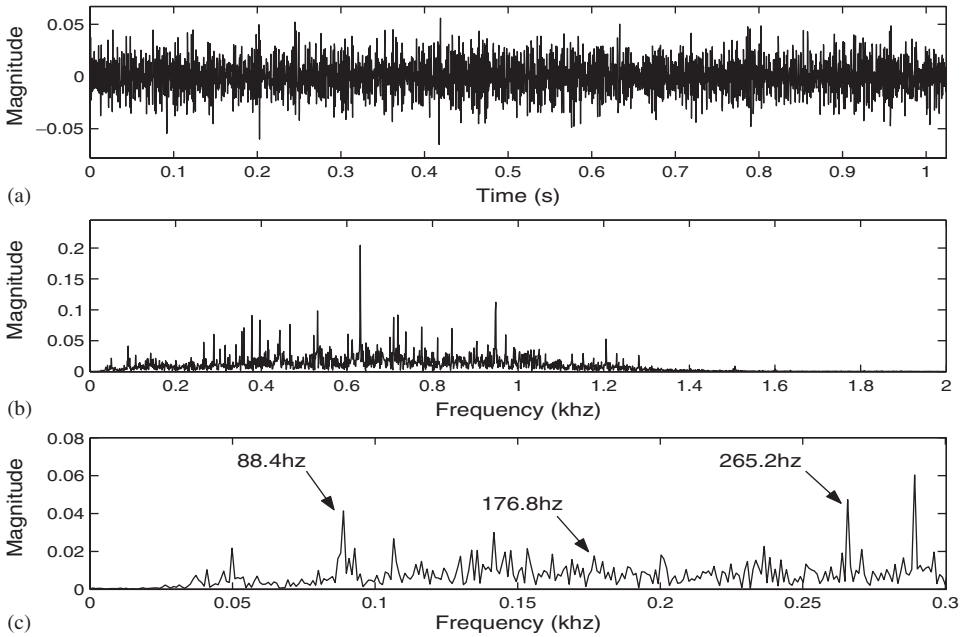


Fig. 9. (a) A vibration signal collected 6 min before the tooth was broken, (b) its Fourier transform, and (c) the zoomed-in plot of the Fourier transform from 0 to 0.3 kHz.

signal, as shown in Fig. 9(c), the composition of the sideband components is rather complicated. It is difficult to recognise the fault directly based on the Fourier transform. Fig. 10(a) shows the first seven IMFs obtained using the BS-EMD. Although, we can more or less observe the transients from the amplitude and phase changes revealed in IMFs 3–6, the features are rather obscure in comparison with those shown in Fig. 6(a) for the signal analysed earlier. However, the Hilbert spectrum, as shown in Fig. 10(b), provides sufficient information for detection of the fault; the time spacing between the neighbouring relatively dark patches is close to the rotation period of the damaged gear or its multiple; and the frequency ranges of the transients cover the sidebands of the meshing frequency of the last gear pair and its second and third harmonics. The IMFs and Hilbert spectrum obtained using the original EMD are shown in Fig. 11. For this signal, the two methods perform comparably and the Hilbert spectrum shows clearly the existence of a localised fault.

The signal is also analysed using CWT. Fig. 12(a) shows the real parts of the CWT at the dyadic scales from $a = 1$ to 64. While these waveforms are less indicative about the fault, the CWT time–frequency representation shown in Fig. 12(b) provides certain information about the existence of the tooth crack. However, compared with the Hilbert spectrum, the main problem of the CWT is again that it cannot properly characterise the sharp structures of the transients for the sidebands below the meshing frequency. This is natural because in general CWT cannot properly represent a signal composed of transients at relatively low frequencies and quasi-stationary components at relatively high frequencies. Such a signal, however, could be generated in a gearbox. The decomposition process of the EMD methods is adapted to the local composition of a signal. They thus do not have the mentioned drawback of CWT.

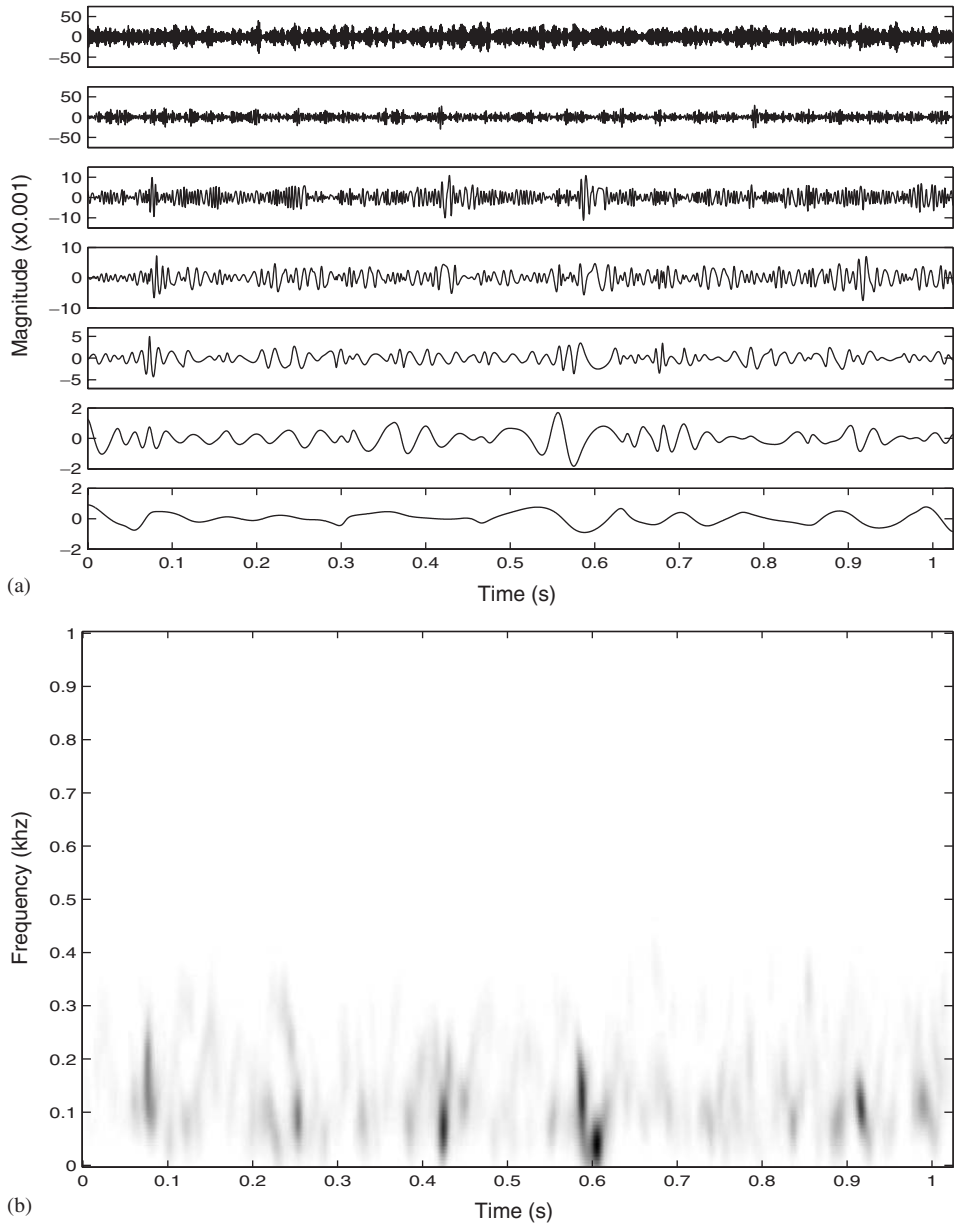


Fig. 10. (a) IMFs of the signal in Fig. 9(a) obtained using BS-EMD. The index of the IMF increases from the top to the bottom. (b) Hilbert spectrum of the 3rd–6th IMFs.

## 5. Conclusion

The empirical mode decomposition and Hilbert spectrum provide a new method for time–frequency analysis and have received great attention in various areas. In this paper, we

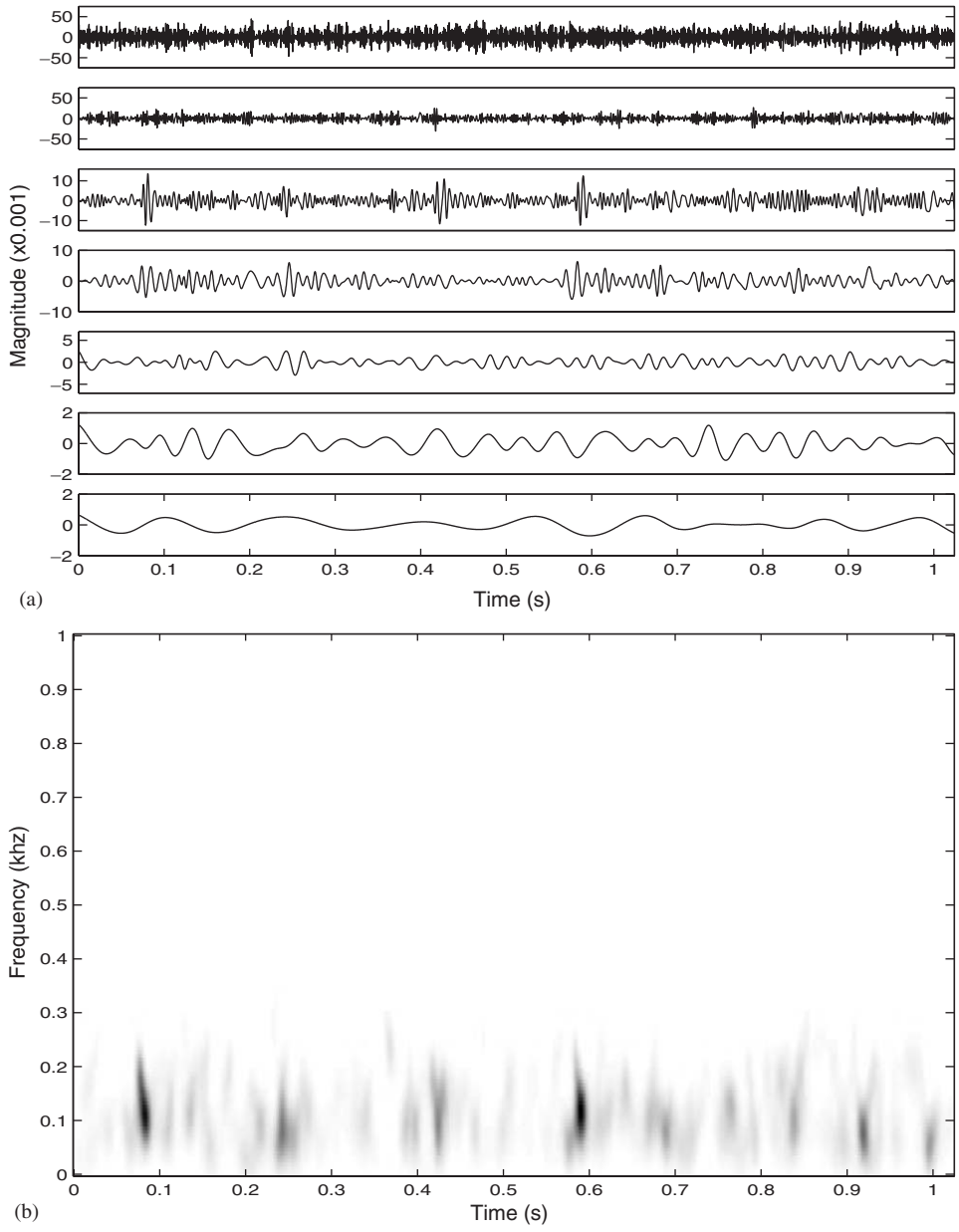


Fig. 11. (a) IMFs of the signal in Fig. 9(a) obtained using the original EMD. The index of the IMF increases from the top to the bottom. (b) Hilbert spectrum of the 3rd–6th IMFs.

applied this method to localised gearbox fault diagnosis. We showed that the B-spline EMD, which is a variation of the original algorithm developed for the convenience of mathematical studies, behaves as a multiscale filter bank. This is of interest to the study of the mechanisms behind EMD. To investigate their effectiveness in the fault diagnosis, we applied the original and

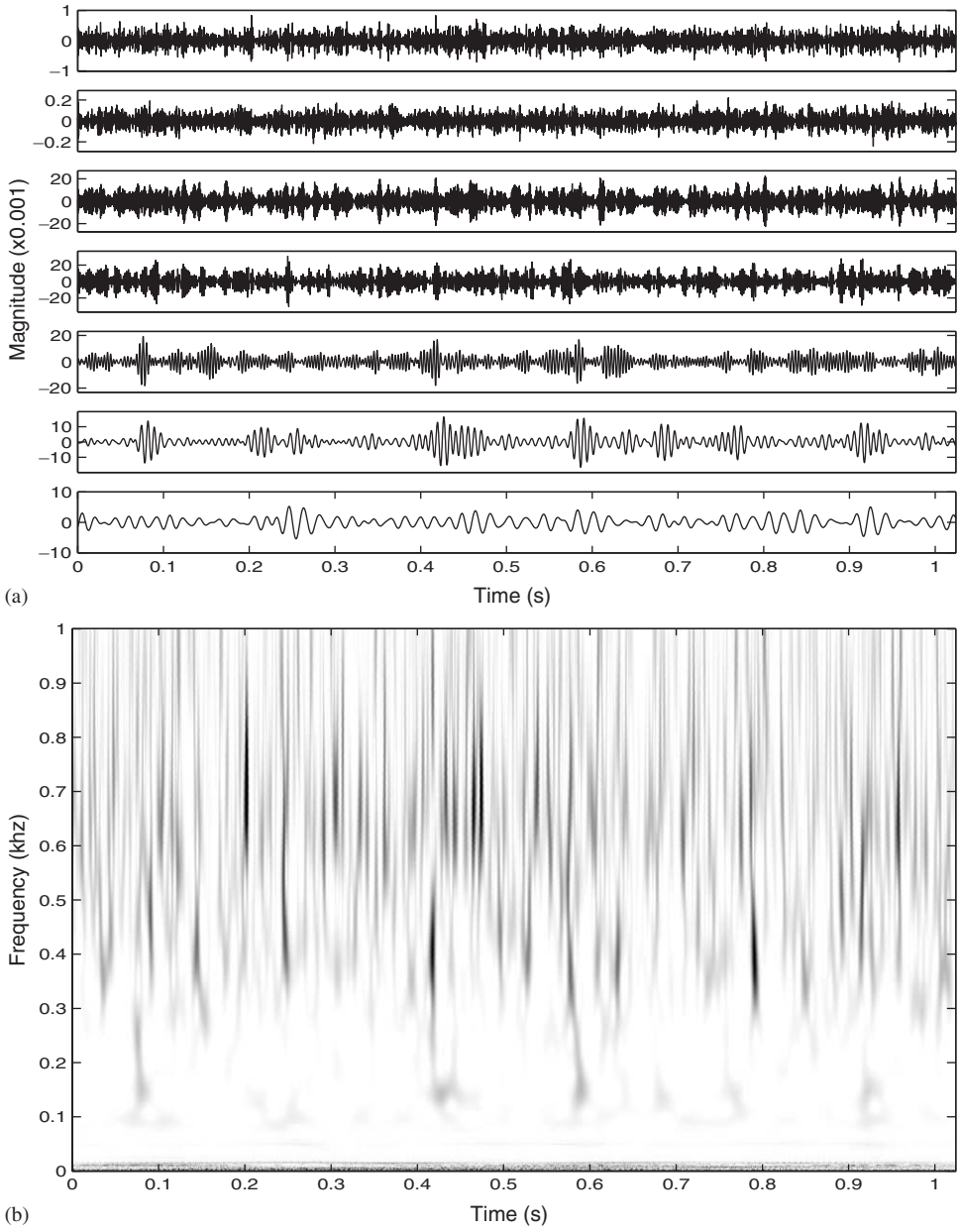


Fig. 12. (a) CWT of the signal in Fig. 9(a) at the dyadic scales from $a = 1$ (top) to 64 (bottom). (b) CWT time–frequency representation.

the B-spline EMD as well as their corresponding Hilbert spectrum to analyse the vibration signals collected from a gearbox with a tooth crack. It was found that the two EMD algorithms and Hilbert spectrum can better enhance the transients excited by the crack than the often used continuous wavelet transform. From a more general point of view, we anticipate that the

empirical mode decomposition and Hilbert spectrum would become an appealing tool in non-stationary vibration signal analysis for diagnosis of localised faults of other mechanical systems.

## References

[1] S. Braun, Mechanical Signature Analysis, Academic Press, London, 1986.
[2] Z.K. Peng, F.L. Chu, Application of the wavelet transform in machine condition monitoring and fault diagnostics: a review with bibliography, Mechanical Systems and Signal Processing 18 (2004) 199–221.
[3] S. Mallat, A Wavelet Tour of Signal Processing, Academic Press, London, 1998.
[4] N.E. Huang, Z. Shen, S.R. Long, N.C. Wu, H.H. Shih, Q. Zheng, N.C. Yen, C.C. Tung, H.H. Liu, The empirical mode decomposition and the Hilbert spectrum for nonlinear and non-stationary time series analysis, Proceedings of the Royal Society of London A 454 (1998) 903–995.
[5] D. Pines, L. Salvino, Health monitoring of one dimensional structures using empirical mode decomposition and the Hilbert–Huang transform, Proceedings of SPIE 4701 (2002) 127–143.
[6] Y. Chen, M.Q. Feng, Technique to improve the empirical mode decomposition in the Hilbert–Huang transform, Journal of Earthquake Engineering and Engineering Vibration, 2003, to appear.
[7] R.R. Zhang, S. Ma, S. Hartzell, Signatures of the seismic source in EMD-based characterization of the 1994 Northridge, California, earthquake recordings, Bulletin of the Seismological Society of America 93 (2003) 501–518.
[8] Q. Chen, N. Huang, S. Riemenschneider, Y. Xu, A B-spline approach for empirical mode decompositions, Advances in Computational Mathematics, 2003, to appear.
[9] L. Cohen, Time–Frequency Analysis, Prentice-Hall, Englewood Cliffs, NJ, 1995.
[10] C. deBoor, A Practical Guide to Splines, Prentice-Hall, Englewood Cliffs, NJ, 1978.
[11] P. Flandrin, F. Rilling, P. Goncaleves, Empirical mode decomposition as a filter bank, IEEE Signal Processing Letters 11 (2004) 112–114.
[12] Z. Wu, N. Huang, A study of the characteristics of white noise using the empirical mode decomposition method, Proceedings of the Royal Society of London A 460 (2004) 1597–1611.